Proceedings of the Fifteenth International Conference on
Computational Structures Technology
Edited by: P. Iványi, J. Kruis and B.H.V. Topping
Civil-Comp Conferences, Volume 9, Paper 10.7
Civil-Comp Press, Edinburgh, United Kingdom, 2024
ISSN: 2753-3239, doi: 10.4203/ccc.9.10.7

Homogenization Based Computational Two-Scale Modelling of Self-Contact in Collapsible Fluid Saturated Micropores

E. Rohan[1] and J. Heczko[2]

[1]Department of Mechanics, NTIS, Faculty of Applied Sciences, University of West Bohemia, Pilsen, Czech Republic
[2]NTIS - New Technologies for the Information Society, Faculty of Applied Sciences, University of West Bohemia, Pilsen, Czech Republic

Abstract

Modelling the unilateral contact due to collapsible pores in porous media presents a challenging nonlinear problem which requires convenient approximations allowing for a tractable numerical solutions. We have derived its two-scale formulation obtained by the homogenization of the fluid-structure interaction at the pore level. We focus on periodic structures with pores distributed as fluid-filled inclusions with narrow parts (fissures) in which the matching contact surfaces are specified. It is demonstrated how the fluid increases the structure stiffness. Two variational formulations of the macroscopic problem are considered; the first one is a nonlinear elastic problem coupled with the local contact problems introduced using a variational inequality, the second one is formulated as a two-scale contact problem with a two-scale contact constraint. To reduce the computational effort, we propose an approximation of the local contact problem solutions using master microproblems solved for selected macroscopic deformations. For this, the sensitivity analysis framework analogical to the one used in the shape optimization is employed.

Keywords: unilateral contact, fluid-saturated porous media, multiscale modeling, homogenization, semi-smooth Newton method, two-scale finite element method

1 Introduction

We consider fluid-saturated poroelastic structures characterized by unilateral self-contact at the pore level of the periodic microstructure. The unilateral frictionless contact interaction is considered on matching pore surfaces of the elastic skeleton. Depending on the deformation due to applied macroscopic loads, the self-contact interaction alters the one between the solid and fluid phases. We derive two-scale model of the homogenized porous medium for the disconnected porosities using the framework of the periodic unfolding homogenization [2,4], *cf.* our previous paper [7] where only empty pores were considered. For the closed fluid-saturated pore microstructures, a nonlinear elastic model is obtained at the macroscopic scale. The derived problem can be adapted for structures with connected porosities admitting for flow; this issue will be subject of a separate paper.

We propose and test new modifications of the original two-scale computational algorithm reported [7] which is based on alternating micro- and macro-level steps. As a novelty, a dual formulation of the pore-level contact problems in the local representative cells provides actual active contact sets which enables to compute consistent effective elastic coefficients at particular macroscopic points. At the macroscopic level, a sequential linearization leads to an incremental equilibrium problem which is constrained by a projection arising from the homogenized contact constraint, such that the Uzawa algorithm can be used. At the local level, the finite element discretized contact problem attains the form of a nonsmooth equation which which is solved using the semi-smooth Newton method [3] without any regularization, or a problem relaxation. Numerical examples of 2D deforming structures are presented.

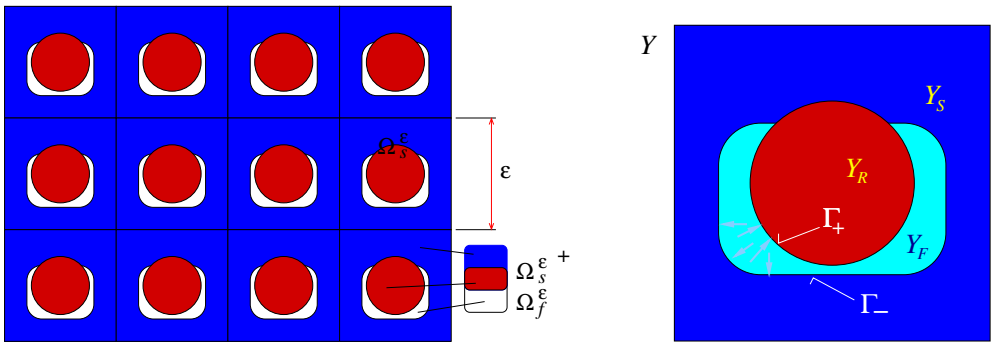

Figure 1: Left: periodic lattice of the porous structure. Right: representative cell Y. Contact surfaces $\Gamma_c^{+/-}$, subparts on the pore surface Γ_{fs}.

2 Problem formulation

In the framework of the unfolding method of homogenization, the limit two-scale models of the unilateral contact in porous structures with disconnected porosity is derived using the asymptotic analysis with respect to heterogeneity scale parameter

$\varepsilon \to 0$. An open bounded domain $\Omega \subset \mathbb{R}^d$, with the dimension $d = 2, 3$, is constituted by the solid elastic skeleton Ω_s^ε and by the fractures (fissures) Ω_f^ε which are saturated by a viscous fluid, so that

$$\Omega = \Omega_s^\varepsilon \cup \Omega_f^\varepsilon \cup \Gamma^\varepsilon \ , \quad \Omega_s^\varepsilon \cap \Omega_f^\varepsilon = \emptyset \ , \quad \overline{\Omega_f^\varepsilon} \subset \Omega \ , \tag{1}$$

where $\Gamma^\varepsilon = \overline{\Omega_s^\varepsilon} \cap \overline{\Omega_f^\varepsilon}$ is the interface; the contact is possible on $\Gamma_c^\varepsilon \subset \Gamma^\varepsilon$. The pores Ω_f^ε and the skeleton are constituted as periodic lattices using domains Y_f and Y_s, respectively, where $Y = Y_s \cup Y_f \cup \Gamma$ is the representative unit cell.

The problem is described by a variational inequality governing the displacements $\boldsymbol{u}^\varepsilon$ and pore pressure p^ε which is defined by constants in each closed pore $\Omega^{k,\varepsilon} \subset \Omega_f^\varepsilon$. The following sets are employed:

$$\begin{aligned} &\textit{kinematic constraint:} \quad \mathcal{K}^\varepsilon = \{\boldsymbol{v} \in \mathbf{H}^1(\Omega_s^\varepsilon) |\ \boldsymbol{v} = 0 \text{ on } \partial_u \Omega_s^\varepsilon \ , \ g_c^\varepsilon(\boldsymbol{v}) \le 0 \ \text{ on } \Gamma_c^\varepsilon\} \ , \\ &\textit{admissible pressure field:} \quad \mathcal{Q}^\varepsilon = \{q \in L^2(\Omega) |\ q \text{ is constant in each } \Omega^{k,\varepsilon} \ , \ k \in I_f^\varepsilon\} \ , \end{aligned}$$

where g_c^ε is the contact gap function. The following system (2) and (3) is to be satisfied by $\boldsymbol{u}^\varepsilon$ and p^ε:

• *Solid equilibrium in Ω_s^ε and pore fluid mass conservation in $\Omega_f^{\varepsilon,k}$,*

$$\begin{aligned} \nabla \cdot \mathbb{D}\boldsymbol{e}(\boldsymbol{u}^\varepsilon) + \boldsymbol{f}^\varepsilon = 0 \quad &\text{in } \Omega_s^\varepsilon \ , \quad \boldsymbol{\sigma}^\varepsilon \cdot \boldsymbol{n} = -p^\varepsilon \boldsymbol{n} \text{ on } \partial\Omega_f^\varepsilon \setminus \Gamma_c^\varepsilon \ , \\ \int_{\partial\Omega_f^{\varepsilon,k}} \boldsymbol{u}^\varepsilon \cdot \boldsymbol{n}^{[\mathrm{s}]} - \gamma \int_{\Omega_f^{\varepsilon,k}} p^\varepsilon = 0 \quad &\text{for each pore } \Omega_f^{\varepsilon,k},\ k = 1, \dots, N^\varepsilon \ . \end{aligned} \tag{2}$$

where $\boldsymbol{e}(\boldsymbol{v}) = (e_{ij}(\boldsymbol{v}))$ is the small strain tensor, γ is the fluid compressibility, $\mathbb{D} = (D_{ijkl})$ is the elasticity tensor, and $\boldsymbol{n}^{[\mathrm{s}]}$ designates the unit normal vector outward to Ω_s^ε.

• *Contact condition* – friction-less contact on Γ_c^ε

$$g_c^\varepsilon(\boldsymbol{u}^\varepsilon) \le 0 \ , \quad \sigma_n^\varepsilon \le -p^\varepsilon \ , \quad g_c^\varepsilon(\boldsymbol{u}^\varepsilon)(\sigma_n^\varepsilon + p^\varepsilon) = 0 \ , \tag{3}$$

The variational formulation reads: Find $\boldsymbol{u}^\varepsilon \in \mathcal{K}^\varepsilon$ and the pressure $p^\varepsilon \in \mathcal{Q}^\varepsilon$ such that (given volume forces $\boldsymbol{f}^\varepsilon$)

$$\begin{aligned} \int_{\Omega_s^\varepsilon} \mathbb{D}\boldsymbol{e}(\boldsymbol{u}^\varepsilon) : \boldsymbol{e}(\boldsymbol{v}^\varepsilon - \boldsymbol{u}^\varepsilon) + \int_{\partial\Omega_f^\varepsilon} p^\varepsilon \boldsymbol{n}^{[\mathrm{s}]} \cdot (\boldsymbol{v}^\varepsilon - \boldsymbol{u}^\varepsilon) \ge \int_{\Omega_s^\varepsilon} \boldsymbol{f}^\varepsilon \cdot (\boldsymbol{v}^\varepsilon - \boldsymbol{u}^\varepsilon) \ , \quad \forall \boldsymbol{v}^\varepsilon \in \mathcal{K}^\varepsilon \ , \\ \int_{\partial\Omega_f^\varepsilon} q^\varepsilon \boldsymbol{u}^\varepsilon \cdot \boldsymbol{n}^{[\mathrm{s}]} - \gamma \int_{\Omega_f^\varepsilon} p^\varepsilon q^\varepsilon = 0 \quad \forall q^\varepsilon \in \mathcal{Q}^\varepsilon \ . \end{aligned} \tag{4}$$

3 Homogenized porous medium with self-contact at the pore level

For the structures with fluid saturated disconnected pores, the homogenized limit problem attains the same form as the one derived for the structures without fluid (empty

pores), although the effective tangent stiffness modulus involved in the incremental formulation reflects the fluid action. Henceforth, we focus on the model describing the quasistatic response of the homogenized medium with disconnected pores. We denote by $\boldsymbol{u}^0$ and p^0 the macroscopic displacement and pressure fields, respectively, and by $\boldsymbol{u}^1$ the fluctuating part of the micro-displacements, being Y-periodic functions in the micro-variable $y \in Y$. The truncated asymptotic expansion is introduced using the unfolding operator $\mathcal{T}_\varepsilon()$, see [1], for $x \in \Omega$ and $y \in Y$,

$$\mathcal{T}_\varepsilon(\boldsymbol{u}^\varepsilon(x)) = \boldsymbol{u}^0(x) + \varepsilon \boldsymbol{u}^1(x,y) + \varepsilon^2(\dots \ . \tag{5}$$

Admissible two-scale displacements must satisfy $\boldsymbol{u}^1 \in \mathcal{K}_Y(\nabla \tilde{\boldsymbol{u}}^0)$ where the set $\mathcal{K}_Y$ is defined using the gap function $g_c^Y(\boldsymbol{u}^1, \nabla \boldsymbol{u}^0) = [\nabla \boldsymbol{u}^0 \widehat{y} + \boldsymbol{u}^1 - \widehat{y}]_n^Y \leq 0$ with $\widehat{y} \in \Gamma_c$, where $\Gamma_c \subset \Gamma_{fs}$ is the contact surface, a part of the pore wall Γ_{fs}. The limit two-scale problem with quasistatic flow is derived from Problem (4). It involves Local problems defined in Y for a.a. $x \in \Omega$, and the Global problem defined in Ω.

The Local problem of the solid in Y_s describes its response to applied macroscopic strain $\boldsymbol{e}_x(\boldsymbol{u}^0)$, being constraint by the unilateral contact on the pore contact surface $\Gamma_c \subset \Gamma_{fs}$ and by the fluid mass conservation in deformed pores $\tilde{Y}_f$,

$$\begin{gathered}
\fint_{Y_s} \mathbb{D}\boldsymbol{e}_y(\boldsymbol{u}^1 + \boldsymbol{\Pi}^{ij} e_{ij}^x(\boldsymbol{u}^0)) : \boldsymbol{e}_y(\boldsymbol{v} - \boldsymbol{u}^1) + p^0 \fint_{Y_s} \nabla_y \cdot (\boldsymbol{v} - \boldsymbol{u}^1) \geq 0 \ , \quad \forall \boldsymbol{v} \in \mathcal{K}_Y(\nabla \boldsymbol{u}^0) \ , \\
\text{whereby} \qquad \phi_f \nabla_x \cdot \boldsymbol{u}^0 - \fint_{Y_s} \nabla_y \cdot \boldsymbol{u}^1 + \gamma \phi_f p^0 = 0 \ ,
\end{gathered} \tag{6}$$

where $\bar{\boldsymbol{u}} := \boldsymbol{\Pi}^{ij} e_{ij}^x(\boldsymbol{u}^0)$ is the affine part of the microscopic displacement field in Y_s produced by the homogeneous strain $\boldsymbol{e}_x(\boldsymbol{u}^0)$ with $\Pi_k^{ij} = \delta_{ik} y_j$. For the global problem in Ω, two formulations are possible. We first describe the straightforward consequence of the two-scale limit problem coupling the displacements $\boldsymbol{u}^0(x)$ and $\boldsymbol{u}^1(x,y)$ through the static equilibrium

$$\int_\Omega \boldsymbol{\sigma}^0(\boldsymbol{u}^0, \boldsymbol{u}^1) : \boldsymbol{e}_x(\boldsymbol{v}^0) - \int_\Omega p^0 \phi_f \nabla_x \cdot \boldsymbol{v}^0 = \int_\Omega \bar{\boldsymbol{f}} \cdot \boldsymbol{v}^0 \quad \forall \boldsymbol{v} \in U_0(\Omega) \ . \tag{7}$$

Although $p^0(x)$ is the macroscopic pore pressure, it can be considered as the microscopic variable. Therefore, p^0 can be eliminated, thus, yielding a nonlinear elastic constitutive law for the homogenized solid. The *Local sub-problem (LP)* reads: Given $\nabla \boldsymbol{u}^0(x)$ at $x \in \Omega$, find $\boldsymbol{u}^1(x,\cdot) \in \mathcal{K}_Y(\nabla \boldsymbol{u}^0)$,

$$\begin{aligned}
&\fint_{Y_s} \mathbb{D}\boldsymbol{e}_y(\boldsymbol{u}^1 + \boldsymbol{\Pi}^{ij} e_{ij}^x(\boldsymbol{u}^0)) : \boldsymbol{e}_y(\boldsymbol{v} - \boldsymbol{u}^1) \\
&+ \frac{1}{\gamma \phi_f} \left(\fint_{Y_s} \nabla_y \cdot \boldsymbol{u}^1 - \phi_f \nabla_x \cdot \boldsymbol{u}^0 \right) \fint_{Y_s} \nabla_y \cdot (\boldsymbol{v} - \boldsymbol{u}^1) \geq 0 \ ,
\end{aligned} \tag{8}$$

for all $\boldsymbol{v} \in \mathcal{K}_Y(\nabla \boldsymbol{u}^0)$. By the consequence of (7), the *Macroscopic – global problem*

(GP) is formulated, as follows Find $(\boldsymbol{u}^0, \boldsymbol{u}^1) \in U_0(\Omega) \times L^2(\Omega; \mathbf{H}^1_{\#}(Y_s))$ which satisfy

$$\int_\Omega \boldsymbol{\sigma}^0(\boldsymbol{u}^0, \boldsymbol{u}^1) : \boldsymbol{e}_x(\boldsymbol{v}^0) - \frac{1}{\gamma\phi_f} \int_\Omega \left(\fint_{Y_s} \nabla_y \cdot \boldsymbol{u}^1 - \phi_f \nabla_x \cdot \boldsymbol{u}^0 \right) \phi_f \nabla_x \cdot \boldsymbol{v}^0 = \int_\Omega \bar{\boldsymbol{f}} \cdot \boldsymbol{v}^0 \ , \tag{9}$$

for all $\boldsymbol{v}^0 \in U_0(\Omega)$. The Sobolev space $\mathbf{H}^1_{\#}(Y_s)$ contains Y-periodic functions, applied also in the "sliding bilateral contact" set defined below.

3.1 Macroscopic Linear (ML) subproblem

The two-scale algorithm proposed in [7] can be adapted. It is based on the linearization of the stress $\boldsymbol{\sigma}^0(\boldsymbol{u}^0, \boldsymbol{u}^1)$, leading to an incremental formulation of the global equilibrium arizing from (9). The macroscopic increment $\delta\boldsymbol{u}^0$ driven by the out of balance are computed with the "fixed sliding contact" constraint due to active contact sets $\Gamma_c^*(x)$ (in the context of a space-discretized formulation, local true contact surfaces are identified at all points $x \in \Omega$ where the microscopic problems are solved). The effective macroscopic tangent stiffness can be defined in terms of perturbations $(\delta\boldsymbol{u}^0, \delta\boldsymbol{u}^1)$ such that $\Gamma_c^*(x)$ is not modified. In other words, the affine displacement field induced in $Y(x)$ by the strain $\boldsymbol{e}_x(\delta\boldsymbol{u}^0(x))$ is compensated by $\delta\boldsymbol{u}^1(x, y)$ with $y \in Y(x)$, such that the active contact associated with the "master surface" is not changed, see [7] for details. For a displacement field $\bar{\boldsymbol{u}} := \boldsymbol{\Pi}^{ij} e^x_{ij}$, induced by any (small) macroscopic strain $\boldsymbol{e}^x$, let us introduce the set of admissible displacement perturbations,

$$V_0(\bar{\boldsymbol{u}}, Y_s^{(t)}, x) = \{\boldsymbol{v} \in \mathbf{H}^1_{\#}(Y_s^{(t)}) |\ [\boldsymbol{v} + \bar{\boldsymbol{u}}]_n^{(t)} = 0 \text{ on } \Gamma_*^{(t)}(x)\} \ . \tag{10}$$

The characteristic microscopic response of the linearized "sliding contact" microstruture is introduced: Find $\boldsymbol{w}^{ij}(x, \cdot) \in V_0(\boldsymbol{\Pi}^{ij}, Y_s, x)$, $i, j = 1, \ldots, d$ which satisfy

$$\fint_{Y_s} \mathbb{D}\boldsymbol{e}_y(\boldsymbol{w}^{ij} + \boldsymbol{\Pi}^{ij}) : \boldsymbol{e}_y(\boldsymbol{v}) + \frac{1}{\gamma\phi_f} \left(\fint_{Y_s} \nabla_y \cdot \boldsymbol{w}^{ij} - \phi_f \delta_{ij} \right) \fint_{Y_s} \nabla_y \cdot \boldsymbol{v} = 0 \ , \tag{11}$$

for all $\boldsymbol{v} \in V_0(0, Y_s, x)$. The global incremental problem is based on the elastic constitutive law involving the tangent stiffness $\mathbb{D}^H = (D^H_{ijkl})$ computed by the following symmetric expression of D^H_{ijkl},

$$\begin{aligned} D^H_{ijkl} = {} & a_{Y_S}\left(\boldsymbol{w}^{ij} + \boldsymbol{\Pi}^{ij},\, \boldsymbol{w}^{kl} + \boldsymbol{\Pi}^{kl}\right) \\ & + \frac{1}{\gamma\phi_f} \left(\fint_{Y_s} \nabla_y \cdot \boldsymbol{w}^{ij} - \phi_f \delta_{ij} \right) \left(\fint_{Y_s} \nabla_y \cdot \boldsymbol{w}^{kl} - \phi_f \delta_{kl} \right) \ . \end{aligned} \tag{12}$$

Incremental formulation. We assume the current approximation $\widetilde{\boldsymbol{u}}^0$ of the macroscopic displacement field, so that $\widetilde{\boldsymbol{u}}^1$ is computed using the local contact problems (8), yielding $\widetilde{\boldsymbol{u}}^1(x, \cdot)$ the local microstructure deformations, hence the true contact set for each microstructure $Y_s(x)$. Small perturbations $\delta\boldsymbol{u}^0$ and $\delta\boldsymbol{u}^1$ are related by

the "linearized" contact problem which yileds the corrector problem (11), whereby $\delta \boldsymbol{u}^1 = \boldsymbol{w}^{ij} e^x_{ij}(\delta \boldsymbol{u}^0)$. Let $r(\boldsymbol{v}^0)$ be the macroscopic out-of-balance functional,

$$r(\boldsymbol{v}^0) := \int_\Omega \boldsymbol{f} \cdot \boldsymbol{v}^0 + \int_{\partial_\sigma \Omega} \boldsymbol{b} \cdot \boldsymbol{v}^0 - \int_\Omega \widetilde{\boldsymbol{\sigma}}^{\rm tot} : \boldsymbol{e}_x(\boldsymbol{v}^0) \ , \tag{13}$$

where $\widetilde{\boldsymbol{\sigma}}^{\rm tot}$ is the current approximation of the total stress $\boldsymbol{\sigma}^{\rm tot} = \boldsymbol{\sigma}^0 - p^0 \phi_f \boldsymbol{I}$ evaluated for the $\widetilde{\boldsymbol{u}}^0$; note that $\widetilde{p}^0$ is determined for $\widetilde{\boldsymbol{u}}^0$ by virtue of $(6)_2$. The perturbations $\delta \boldsymbol{u}^0 \in U(\Omega)$ satisfy

$$\int_\Omega \mathbb{D}^H \boldsymbol{e}_x(\delta \boldsymbol{u}^0) : \boldsymbol{e}_x(\boldsymbol{v}^0) = r(\boldsymbol{v}^0) \ , \quad \forall \boldsymbol{v} \in U_0(\Omega) \ . \tag{14}$$

Then the stress is updated, $\boldsymbol{\sigma}^{\rm tot} := \widetilde{\boldsymbol{\sigma}}^{\rm tot}(\widetilde{\boldsymbol{u}}^0) + \delta \boldsymbol{\sigma}^{\rm tot}$ with $\delta \boldsymbol{\sigma}^{\rm tot} := \mathbb{D}^H \boldsymbol{e}_x(\delta \boldsymbol{u}^0)$ involving the tangential stiffness effective modulus $\mathbb{D}^H$. The displacement field for the new iteration is updated, $\tilde{\boldsymbol{u}}^0 := \boldsymbol{u}^0 + \delta \boldsymbol{u}^0$ in Ω. Solving of the microproblem (8) and the macro-problem (14) repeats until the convergence is attained, *i.e.* $\|\delta \boldsymbol{u}^0\|$ is sufficiently small.

3.2 Macroscopic Contact (MC) method

The direct convergence result yields a variational inequality involving both $\boldsymbol{u}^0$ and $\boldsymbol{u}^1$. Therefore, it is not obvious to retain the "contact problems" to be solved at the micro-level only. In [8], the so-called "Macroscopic contact method" has been proposed and tested on microstructures with drained pores. Here we apply this method to solve the homogenized contact problems for fluid-saturated porous structures Using the local true contact surfaces $\Gamma_c^*(x)$ determined at microstructures $\widetilde{\mathcal{M}}_Y(x)$, the following sets are introduced,

$$\begin{aligned} \Sigma_\Gamma &= \{(x,y) \in \mathbb{R}^d \times \mathbb{R}^d |\ y \in \Gamma_c \subset \Gamma_c^*(x),\ x \in \Omega\} \ , \\ \widetilde{\mathcal{K}}^E_\Omega &= \{\boldsymbol{v} \in U_0(\Omega) |\ \widetilde{g}^E_c(\boldsymbol{v}) \le 0 \text{ a.e. in } \Sigma_\Gamma\} \ , \end{aligned} \tag{15}$$

noting that Σ_Γ is a subset of the Cartesian product $\Omega \times \Gamma_c$ Macroscopic equilibrium involving increment $\delta \boldsymbol{u} \in U_0(\Omega)$, and the "micro-macro Lagrange multiplier", λ, describing the "two-scale" contact stress on Σ_Γ, must satisfy

$$\int_\Omega \left(\mathbb{D}^E \boldsymbol{e}_x(\delta \boldsymbol{u}) + \widehat{\boldsymbol{P}}^* \hat{\lambda} \right) : \boldsymbol{e}_x(\boldsymbol{v}) = \int_\Omega \boldsymbol{f} \cdot \boldsymbol{v} - \int_\Omega \tilde{\boldsymbol{\sigma}} : \boldsymbol{e}_x(\boldsymbol{v}) \ , \quad \forall \boldsymbol{v} \in U_0(\Omega) \ , \tag{16}$$

involving adjoint $\widehat{\boldsymbol{P}}^*$ of the gap operator $\widehat{\boldsymbol{P}}$ defined on the two-scale surfaces $\Sigma_\Gamma = \Omega \times \Gamma_c$ and a consistent tangent $\mathbb{D}^E$, and the projection, attaining the form of a nonsmooth equation:

$$0 = \max\{-\hat{\lambda}, \widehat{\boldsymbol{P}} : \boldsymbol{e}_x(\hat{\boldsymbol{u}}) + \widetilde{s}\} \quad \text{ a.e. in } \Sigma_\Gamma \ .$$

Tensor $\mathbb{D}^E$ is introduced using (11) and (12), however, the prescribed sliding contact is restricted to a subdomain of the true contact surfaces. It means that the unilateral contact is verified by $\delta \boldsymbol{u}$ in the global step involving all the microstructures (in the context of the FE discretization) for "nearly semiactive" parts of the contact srfaces $\Gamma_c(x)$ Contact stress $\sim \hat{\lambda}$ defined on Σ_Γ.

4 Numerical examples

To illustrate the derived homogenized model of the porous fluid saturated material with self-contact at the pore level, we consider three issues. The first one is related to the effective stiffness of the deforming elastic material depending on the deformation. The other two are related to the solution of the two-scale nonlinear problem; the two methods, as introduced in sections 3.1 and 3.2 are presented in examples with two different macroscopic loadings. Finally, some perspective of the model order reduction in terms of reducing the number of local problems to be solved are illustrated.

4.1 Tangent stiffness

The tangent stiffness $\mathbb{D}^H(x, \boldsymbol{e}^0)$ characterizes the deformed microstructure at macroscopic positions $x \in \Omega$. We recall that the nonlinearity of the effective elasticity is due to the unilateral contact constraint, although the solid deformation in Y_s is driven by the linear kinematics and the linear Hooke's law. The numerical example shows the verification of the stiffness components D^H_{ijkl} using an approximation based on the effective stress finite differences.

A microscopic cell with circular inclusion was used (see Fig. 3). Its solid part was modelled using Young's modulus $E = 2.3\,\mathrm{GPa}$ and Poisson ratio $\nu = 0.3$ under the assumption of plane strain while the bulk modulus of the fluid was $K = 2.2\,\mathrm{GPa}$. The freely chosen parameters of a comparison are: macroscopic strain $\mathbf{e}^0$, its variation Δe^0, and a small scalar $\delta > 0$.

The slopes of the stress-strain curves are evaluated using tangent stiffness (TS), see (12), and finite differences (FD) computed using the macroscopic stress based on the local problem solution, see (8),

$$d\sigma_{\mathrm{TS}} = D^H_{ijkl}\,\Delta e^0_{kl}\ , \quad d\sigma_{\mathrm{FD}} = \frac{1}{2}\frac{\sigma(\mathbf{e}^0 + \delta\,\Delta\mathbf{e}^0) - \sigma(\mathbf{e}^0 - \delta\,\Delta\mathbf{e}^0)}{\delta}\ . \tag{17}$$

The slopes $d\sigma_{\mathrm{FD}}$ and $d\sigma_{\mathrm{SA}}$ agree for each component.

Fig. 2 shows the results of these comparisons. The quantities shown are: stress components (σ_{11}, σ_{22}, and σ_{12}) and fluid pressure (p_0), slopes of stress components, and true contact boundary Γ^* relative to contact boundaries Γ^+ and Γ^-. The parameters were chosen as:

$$\mathbf{e}^0 = \mathbf{0}\ , \quad \Delta\mathbf{e}^0 = \begin{bmatrix} -0.3 & 0 \\ 0 & 1 \end{bmatrix}\ , \quad \delta \in \langle -0.05, 0.05 \rangle\ . \tag{18}$$

4.2 Solving the macroscopic problems

Solutions of two global problems are presented here, the following definitions apply to both. The macroscopic domain is a square, $x \in \Omega = [0,1] \times [0,1]$, meshed by

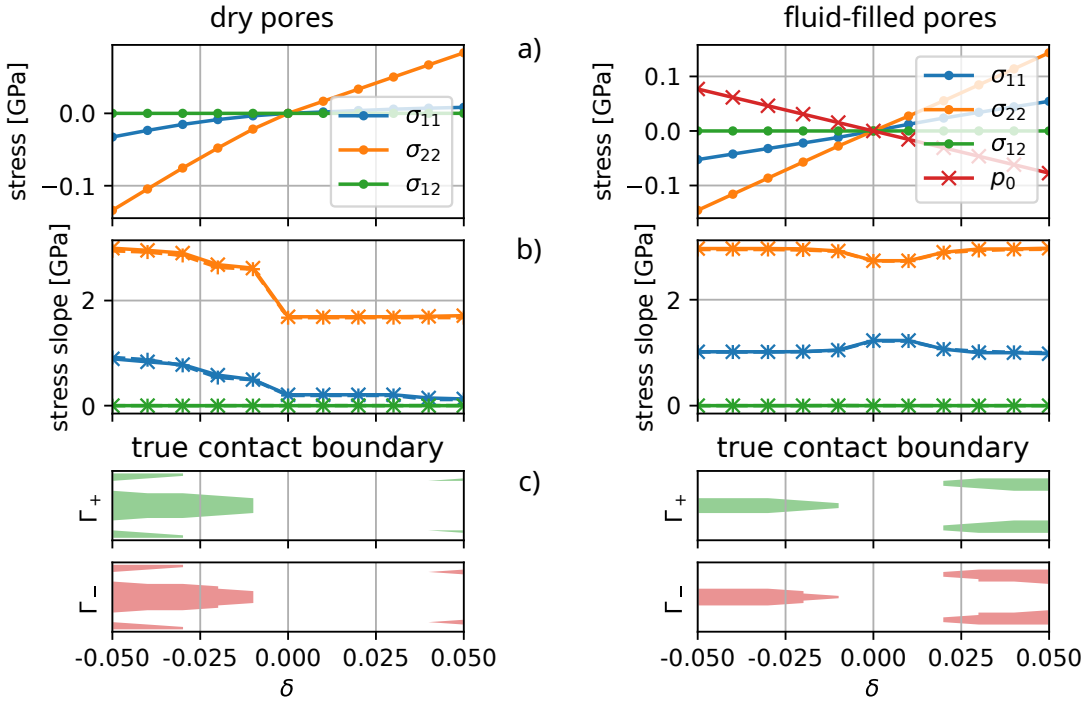

Figure 2: Comparison of tangent stiffness according to (17) with macroscopic strain prescribed as in (18). Stress components (a), their slope (b), and true contact boundary (c); left: dry pores, right: fluid-filled pores.

an array of 4×4 four-node quadrilateral elements with bilinear approximation of displacement.The subsets used for defining boundary conditions were:

$$\begin{aligned} \Gamma_{\text{bottom}} &= \{x |\ x_1 \in [0,1]\ , x_2 = 0\}\ , \\ \Gamma_{\text{top}} &= \{x |\ x_1 \in [0,1]\ , x_2 = 1\}\ . \end{aligned} \tag{19}$$

The macroscopic linear (ML) and the method of macroscopic contact (MC) were compared.

4.2.1 Uniaxial compression

All displacements are fixed at the bottom edge, and a vertical traction is prescribed at the top edge:

$$\begin{aligned} u_1 = u_2 = 0 \quad &\text{on } \Gamma_{\text{bottom}}\ , \\ \boldsymbol{f} = [0, -0.20\,\text{GPa}]^{\text{T}} \quad &\text{on } \Gamma_{\text{top}}\ . \end{aligned} \tag{20}$$

The microscopic domain Y is shown in Fig. 3.

Convergence parameters of the global algorithms are shown in Fig. 4. The method of macroscopic contact (MC) converges faster in terms of both residual r and step length $\delta\boldsymbol{u}$. The non-zero values of λ appear at steps in which the contact term of MC was non-zero, i.e. the state of contact changed in that increment.

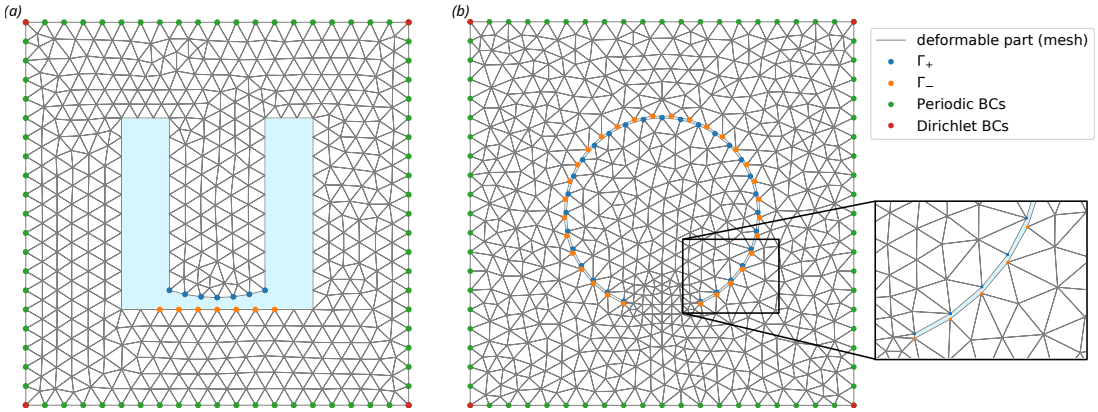

Figure 3: Finite element meshes of the microscopic periodic cell; (a) uniaxial, (b) with circular inclusion.

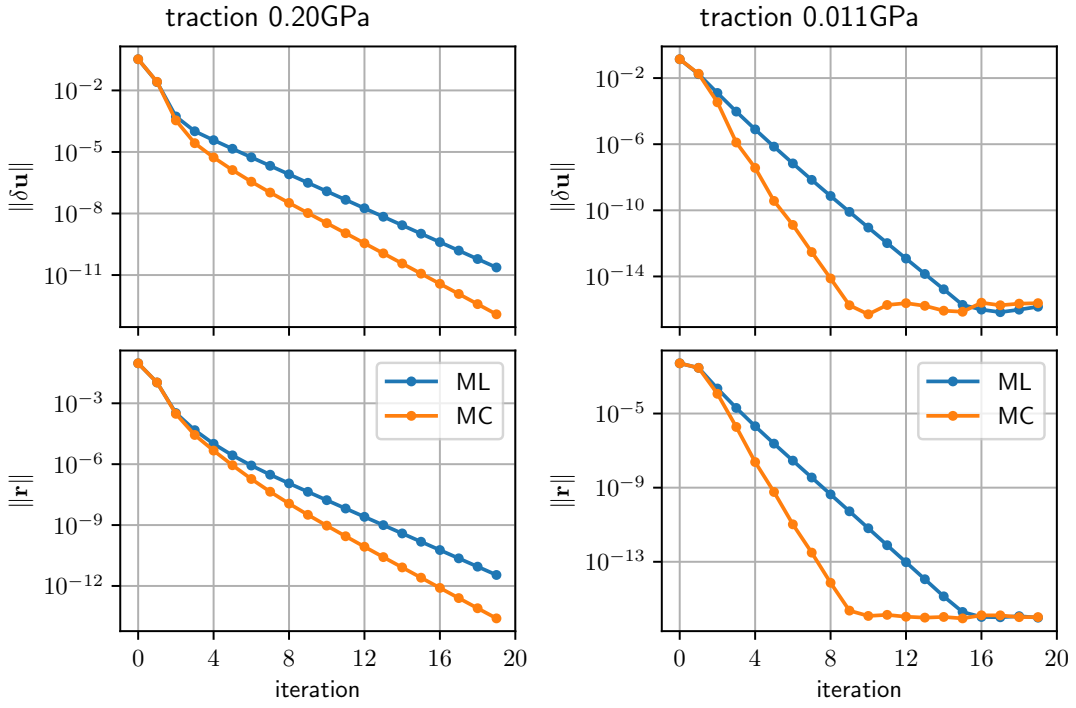

Figure 4: Convergence of the global algorithm; left: uniaxial compression, right: cantilever bending.

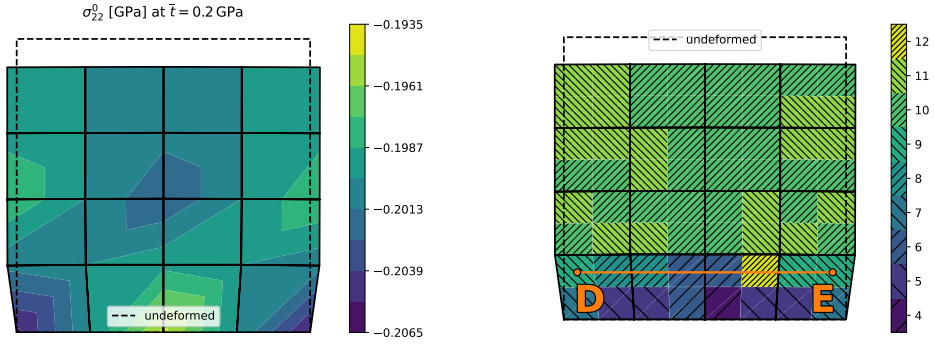

Figure 5: Uniaxial compression: effective stress (vertical component) and number of contact nodes.

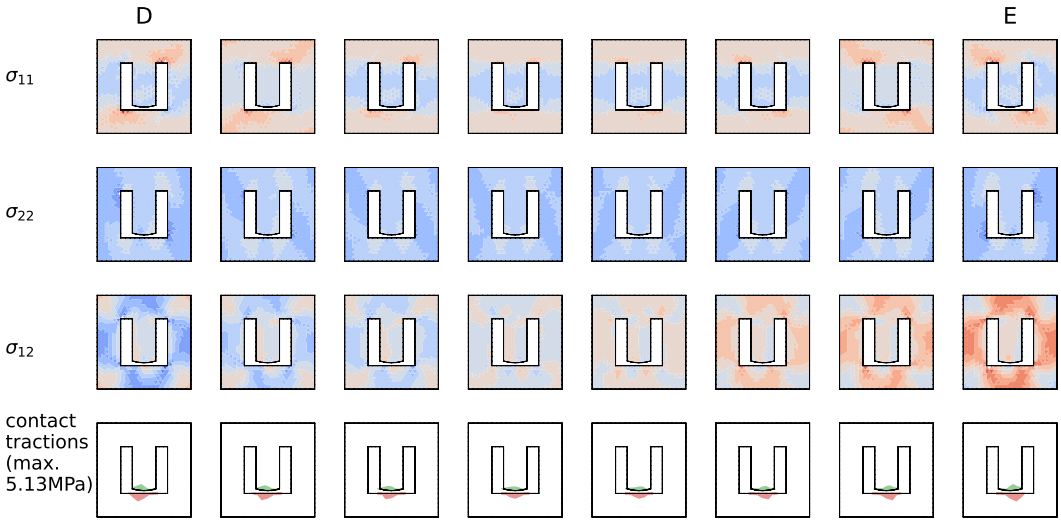

Figure 6: Uniaxial compression: micro-solutions along the D-E line.

In Fig. 5, the macroscopic response is illustrated in terms of the spatial distribution of effective stress, fluid pressure, and the contact status in terms of number of contact nodes. Solutions of selected micro-problems is displayed in terms of the stress components in Y_s and contact tractions on Γ_c, see Fig. 6.

4.2.2 Cantilever bending

All displacements are fixed at the bottom edge, and a horizontal traction is prescribed at the top edge:

$$\begin{aligned} u_1 = u_2 = 0 \quad &\text{on } \Gamma_{\text{bottom}} \,, \\ \boldsymbol{f} = [0.011\,\text{GPa}, 0]^{\text{T}} \quad &\text{on } \Gamma_{\text{top}} \,. \end{aligned} \tag{21}$$

The microscopic domain Y is shown in Fig. 3.

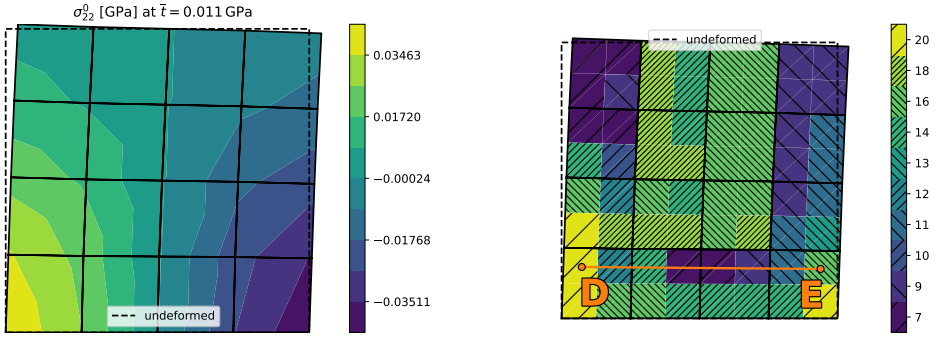

Figure 7: Cantilever bending: Effective stress (vertical component) and number of contact nodes.

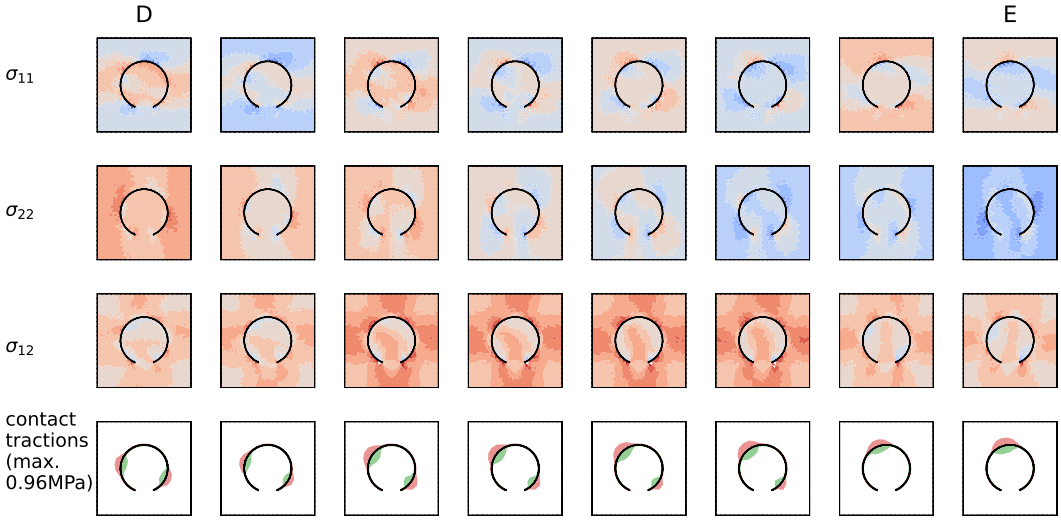

Figure 8: Cantilever bending: micro-solutions along the D-E line.

Convergence parameters of the global algorithms are shown in Fig. 4. Again, the method of macroscopic contact (MC) converges faster in terms of both residual r and step length $\delta \boldsymbol{u}$. In this case, however, λ remains zero in all steps.

Fig. 7 shows spatial distribution of effective stress, fluid pressure, contact status in terms of number of contact nodes, whereas solutions of selected micro-problems are illustrated in Fig. 6, where the stress components and contact normal stress is depicted.

4.3 Approximation in strain space

Problems described above demonstrate the typical feature of the nonlinear two-scale problem leading to the well-known "FE-square" complexity of the numearical algorithm. A possible model order reduction is to reduce the number locally solved contact

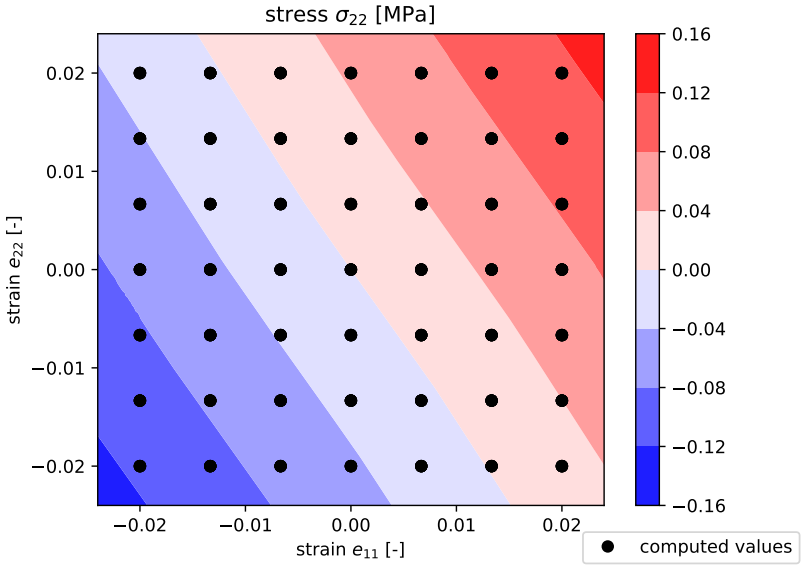

Figure 9: Approximation of the vertical component of effective stress at $e_{12} = 0$.

problems in Y_s for the specific macro-strains, $\boldsymbol{e}(\boldsymbol{u}^0(x))$ at $x \in \Omega$.

A piecewise linear approximation in strain space has been used to reduce the computational cost of solving the global problems. The above described problem of cantilever bending was solved by the ML algorithm with the values of effective stress and tangent stiffness being approximated. Solutions of local problems were pre-computed on a grid spanning the selected interval (see Fig. 9) $[e^0_{11}, e^0_{22}, e^0_{12}]^{\mathrm{T}} \in I_{11} \times I_{22} \times I_{12}$ with $I_{11} = I_{22} = I_{12} = \langle -0.02, 0.02 \rangle$. The grid had $7 \times 7 \times 5$ points, which leads to 245 local problems. Since a single iteration of the global problem requires 64 local problems to be solved, the approximation becomes advantageous after four iterations. An adaptive or more informed strategy of creating the approximation would most probably reduce the total number of local problems and decrease the approximation error. The global results, however, agree well with the full solution in terms of displacement and residual, see Fig. 10.

5 Concluding remarks

We have presented the model of poroelastic fluid saturated medium with unilateral contact on deforming pore surfaces. The model was derived by the homogenization method, assuming local periodicity of the microstructure and disconnected pores, so that flow in the individual, mutually separated pores is not considered. As expected, the fluid-filled pores lead to more constrained setting, which effectively stiffens the response in both compression and tension compared to dry pores. Two solution methods were proposed and tested to solve the two-scale (global) problem. The MC global algorithm achieves a faster rate of convergence in general, as compared to the ML one.

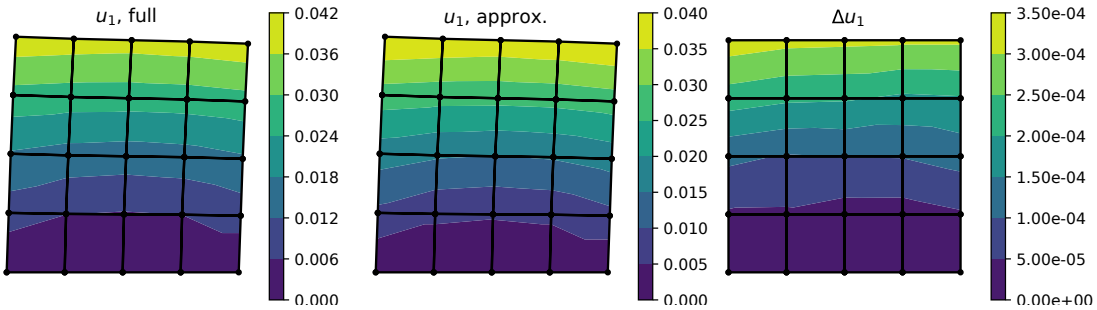

Figure 10: Horizontal component of macroscopic displacement and the difference between full solution (ML) and the solution based on piecewise linear approximation of local results.

This effect is more pronounced with fluid-filled pores. The approximation in strain space offers a substantial reduction in computing time at the cost of approximation error. However, the approach presented here is in an early stage of development and significant improvement is expected. The further research will focus on this issue of the "model order reduction". Besides, the algorithms will be implemented for 3D microstructures which enable for flow in the connected porosity. The proposed model is convenient also to describe mechanics in fractured media, or debonding in composite materials, *cf.* [5]. To solve the contact problem at the microlevel, methods used in the contact mechanics can be employed, see *e.g.* [6].

Acknowledgements

The research has been supported by the grant project GA 22-00863K of the Czech Science Foundation.

References

[1] D. Cioranescu, A. Damlamian, G. Griso. The periodic unfolding method in homogenization. SIAM Journal on Mathematical Analysis, 40(4):1585–1620, 2008.

[2] D. Cioranescu, A. Damlamian, J. Orlik. Homogenization via unfolding in periodic elasticity with contact on closed and open cracks. Asymptotic Analysis, 82(3-4):201–232, 2013.

[3] T. De Luca, F. Facchinei, C. Kanzow. A semismooth equation approach to the solution of nonlinear complementarity problems. Mathematical Programming, 75(3):407–439, 1996.

[4] G. Griso, A. Migunova, J. Orlik. Homogenization via unfolding in periodic layer with contact. Asymptotic Analysis, 99(1-2):23-52, 2016.

[5] S. Marfia, E. Sacco. Computational homogenization of composites experiencing plasticity, cracking and debonding phenomena, Computer Methods in Applied Mechanics and Engineering, 304, 319-341, 2016.

[6] A. Popp. State-of-the-Art Computational Methods for Finite Deformation Contact Modeling of Solids and Structures. In: Popp, A., Wriggers, P. (eds) Contact Modeling for Solids and Particles. CISM International Centre for Mechanical Sciences, vol 585. Springer, 2018.

[7] E. Rohan, J. Heczko. Homogenization and numerical modelling of poroelastic materials with self-contact in the microstructure. Computers and Struct. 230 (2020) 106086.

[8] E. Rohan, J. Heczko. Homogenization and numerical algorithms for two-scale modelling of porous media with self-contact in micropores. Jour. Computat. and Appl. Math., 432, 115276, 2023.

[9] E. Rohan, V. Lukeš. Modeling nonlinear phenomena in deforming fluid-saturated porous media using homogenization and sensitivity analysis concepts. Applied Mathematics and Computation, 267:583–595, 2015.